Differential Metabolic and Multi-tissue Transcriptomic Responses to Fructose Consumption among Genetically Diverse Mice

Guanglin Zhang[1], Hyae Ran Byun[1], Zhe Ying[1], Yuqi Zhao[1], Jason Hong[1], Le Shu[1], Fernando Gomez-Pinilla[1,2]*, Xia Yang[1]*

[1]Department of Integrative Biology and Physiology, University of California, Los Angeles, Los Angeles, California 90095, USA

[2]Department of Neurosurgery, UCLA Brain Injury Research Center, University of California, Los Angeles, Los Angeles, California 90095, USA

Correspondence:

Xia Yang, Ph.D.

Department of Integrative Biology and Physiology

University of California, Los Angeles

Los Angeles, CA 90095, USA

Phone: +1-310-206-1812

Email: xyang123@ucla.edu

Fernando Gomez-Pinilla, Ph.D.

Department of Neurosurgery and Department of Integrative Biology and Physiology

University of California, Los Angeles

Los Angeles, CA 90095, USA

Phone: +1-310-206-9693

Email: fgomezpi@ucla.edu

Abstract

The escalating prevalence of metabolic syndrome (MetS) poses significant risks to type 2 diabetes mellitus, cardiovascular diseases, and non-alcoholic fatty liver disease. High fructose intake has emerged as an environmental risk for MetS and the associated metabolic diseases. To examine inter-individual variability in MetS susceptibility in response to fructose consumption, here we fed three inbred mouse strains, namely C57BL/6J (B6), DBA (DBA) and FVB/NJ (FVB) with 8% fructose in drinking water for 12 weeks. We found that fructose-fed DBA mice had significantly higher amount of body weight, adiposity, and glucose intolerance starting from the 4^{th} week of fructose feeding compared to the control group, while B6 and FVB showed no differences in these phenotypes over the course of fructose feeding. In addition, elevated insulin levels were found in fructose-fed DBA and FVB mice, and cholesterol levels were uniquely elevated in B6 mice. To explore the molecular underpinnings of the observed distinct phenotypic responses among strains, we applied RNA sequencing to investigate the effect of fructose on the transcriptional profiles of liver and hypothalamus tissues, revealing strain- and tissue-specific patterns of transcriptional and pathway perturbations. Strain-specific liver pathways altered by fructose include fatty acid and cholesterol metabolic pathways for B6 and PPAR signaling for DBA. In hypothalamus tissue, only B6 showed significantly enriched pathways such as protein folding, pancreatic secretion, and fatty acid beta-oxidation. Using network modeling, we predicted potential strain-specific key regulators of fructose response such as *Fgf21* (DBA) and *Lss* (B6) in liver, and *Fmod* (B6) in hypothalamus. We validated strain-biased responses of *Fgf21* and *Lss* to fructose in primary hepatocytes. Our findings support that fructose perturbs different tissue networks and pathways in genetically diverse mice and associates with distinct features of metabolic dysfunctions. These results highlight individualized molecular and metabolic responses to fructose consumption and may help guide the development of personalized strategies against fructose-induced MetS.

Introduction

One of the most fascinating questions in biomedical research is why individuals react differently to the same challenge or treatment. In turn, understanding the mechanisms involved in individual variability is crucial for the development of personalized treatments. Metabolic challenges are among the most powerful driving forces of biological adaptations, with long-lasting consequences on homeostatic control and disease stages. Here we investigated the influence of fructose consumption on metabolic and genomic responses across three inbred mouse strains to examine the variability in fructose response as well as the connection between genes and phenotypes, as interactions between environmental factors and host genome or epigenome likely explain the variability.

High fructose consumption is increasingly recognized as a risk factor for the escalating prevalence of metabolic syndrome (MetS) worldwide, posing significant risk for type 2 diabetes mellitus (T2DM), cardiovascular diseases (CVD) and non-alcoholic fatty liver disease [1, 2]. Specifically, high intake of fructose is associated with body weight gain, high blood pressure, cardiovascular diseases [3-5] , insulin resistance [6] and increased plasma triglyceride [7]. Fructose is primarily consumed via beverages and food containing high-fructose corn syrup (HFCS). Human epidemiological studies have established strong connections between consumption of HFCS and metabolic diseases [6, 8-12]. It is already demonstrated that various mouse strains respond differentially to fructose ingestion [13]. However, the difference of molecular changes in response to fructose among individuals with diverse genetic background still remain unclear. To this end, we systematically examine the metabolic parameters and tissue-specific gene regulation in response to fructose treatment in multiple inbred mouse strains. Here we choose to study C57BL/6J (B6), DBA/2J (DBA), and FVB/NJ (FVB) due to their divergence in genetic composition and their previously demonstrated differences in response to a high fat diet [14].

To explore the molecular pathways involved in fructose-induced metabolic challenges, we focused our genomic studies on hypothalamus and liver tissues based on their critical roles in metabolic regulation. The hypothalamus is a critical master regulator of nutrient sensing, food intake, energy expenditure, body weight, and glucose metabolism [15, 16]. Hypothalamic neurons, particularly those in the arcuate nucleus (ARC) and ventromedial hypothalamus (VMH), modulate their activity acutely in response to fluctuations in the levels of metabolic fuels, such as glucose and free fatty acids [17]. The sensing of both glucose and lactate by the hypothalamus

also modulates hepatic lipid metabolism, as intracerebroventricular (ICV) administration of glucose or lactate lowers circulating lipid concentrations and hepatic triglyceride synthesis. Our recent study of the fructose effect on the hypothalamus in a rat model indicate hypothalamus is sensitive to fructose consumption as well as indicated by the increase in the expression of the fructose transporter Glut5 and numerous genes involved in diverse functions [18]. The liver is a main regulator of peripheral metabolism, particularly glucose, steroid, and lipid metabolism. Additionally, fructose is primarily metabolized in the liver, and MetS is closely related with abnormal hepatic metabolism. One of the potential consequences of fructose metabolism in liver is *de novo* triglyceride synthesis by converting dihydroxyacetone phosphate (DHAP) and glyceraldehydes 3-phosphate (GA3P) to glycerol 3-phosphate and pyruvate, respectively [19]. Here, by studying genetically divergent mouse strains, we report that fructose has differential effects on transcriptional alterations in liver and hypothalamus across strains, which provides insights to uncover fundamental mechanisms underlying the individual responses to the metabolic perturbations carried by fructose.

Materials and methods

Animal and experimental design

Male DBA, B6 and FVB mice (Jackson Laboratory) of 7 weeks old weighing 20-25 g were randomly assigned to 8% fructose treatment (n=8-12, 8% w/v fructose in the drinking water) and control group (n=8-10, drinking water) for 14 weeks. We chose 8% fructose to mimic the average fructose consumption found in sugar-sweetened beverages (~10% w/v) consumed in humans. Mice had free access to water and diets and were maintained under standard housing condition (room temperature 22-24 ℃) with 12 h light/dark cycle. Daily food and drink intake were monitored on per-cage basis. The mice were examined for changes in metabolic phenotypes including body weight, body fat, lean mass, intraperitoneal glucose tolerance test (IPGTT), and serum levels of insulin, glucose, total cholesterol (TC), high density lipoprotein cholesterol (HDL), un-esterified cholesterol, free fatty acids (FFA), and triglycerides (TG), as detailed in the following sections. Mice were sacrificed at the end of the 14-week fructose treatment experiment, and hypothalamus and liver tissues were dissected out, flash frozen and stored at −70°C until use.

Body weight and body mass composition

Body weight was measured weekly and body mass composition was determined by NMR in a Bruker mimispec series mq10 machine (Bruker BioSpin, Freemont, CA).

IPGTT

The animals were fasted overnight by transferring mice to clean cages before IPGTT test. The body weight of mice was measured. Volume of 20% glucose (ul) (2g glucose/kg body weight) calculated by 10×body weight (g) was injected intraperitoneally to each mouse at 1st, 4th, 9th and 12th week of fructose treatment. Blood glucose levels from tail vein were measured at 0, 15, 30, 90, and 120 min using an AlphaTrak portable blood glucose meter (Abbott Laboratories, North Chicago, IL, USA). Area under the curve (AUC) was calculated to measure the degree of the glucose tolerance impairment.

Lipids

Mice were fasted overnight before sacrifice at 14th week of fructose, and blood samples were collected through retro-orbital bleeding. Serum TC, HDL, UC, TG, FFA, and glucose were measured by enzymatic colorimetric assays at UCLA GTM Mouse Transfer Core as previously described [18]. Low density lipoprotein cholesterol (LDL) was calculated using the formula: LDL = TC - HDL - (TG/5).

RNA sequencing and data analysis

Total RNA was extracted from hypothalamus and liver using All-Prep DNA/RNA/miRNA Universal Kit (Qiagen, CA. USA) according to the manufacturer's instructions, including treatment with DNase I. RNA quality was evaluated with Agilent 2100 Bioanalyzer (Agilent Technologies, CA, USA). All RNA samples had RNA integrity number (RIN) over 8. Sequencing libraries were prepared using Illumina TruSeq Stranded Total RNA with Ribo-Zero Gold Library Prep kit. Libraries were sequenced in pair-end mode on an Illumina HiSeq 4000 sequencing system. To identify the differentially expressed genes and transcripts, we employed the pipeline comprised of HISAT, StringTie and Ballgown [20]. HISAT was used to align the RNA-seq reads to a genome [21]; StringTie assembles the alignments into transcripts [22]; Ballgown determines the differential gene expression (DEG) of transcripts after filtering genes with low expression levels (FPKM < 1) using linear model test [23]. Multiple testing was corrected using q value approach to estimate false discovery rate (FDR) and $q < 0.05$ was used to determine significant DEGs. DEGs with $q < 0.05$ from RNAseq data were chosen for pathway enrichment analysis using Database for Annotation, Visualization and Integrated Discovery

(DAVID) [24]. GOTERM_BP_DIRECT, KEGG PATHWAY and REACTOME_PATHWAY was selected for the pathway enrichment. Either of Bonferroni, Benjamini and FDR in which *p* is less than 0.05 was considered as significant.

Identification of key drivers of fructose DEG signature genes

Mergeomics [25] was employed to investigate the gene-gene interaction among the fructose DEG signature genes in B6, DBA and FVB and to identify key perturbation points. Previously constructed gene regulatory Bayesian networks of hypothalamus and liver were used in the analysis. For fructose DEG from each tissue of each mouse strain, we used the weighted key driver analysis (wKDA) in Mergeomics to retrieve the potential key drivers whose network neighborhoods are significantly enriched for fructose DEGs. wKDA takes gene set G (i.e. fructose DEGs) and directional gene network N (i.e. BNs) as inputs. For every gene K in network N, neighboring genes within 1-edge distance were tested for enrichment of genes in G using a chi-square like statistics followed by FDR assessment by permutation. Network genes that reached FDR < 0.05 were reported as potential KDs. The gene subnetworks of key drivers including nodes representing the key drivers and their direct network neighboring genes as well as edges representing the connections between genes were visualized using Cytoscape [26].

Validation of strain-specificity of liver key driver genes of fructose response using primary hepatocyte cell culture

We tested whether two select strain-specific liver network key drivers predicted, namely *Fgf21* for DBA and *Lss* for B6 indeed show strain-specific response, primary hepatocytes were isolated from male B6 and DBA mice of 12 weeks of age. Briefly, each mouse was perfused at a rate of 4.5 ml/minute through port vein with perfusion medium (GIBCO 17701-038) for 5 minutes. Then perfusion medium was replaced by digestion medium containing collagenase (GIBCO 17703-034) for another 7 minutes. The liver was torn into pieces, filtered and pelleted down at 50g for 3 minutes at 4°C, followed by the addition of 20 ml 40% cold percoll and centrifugation at 200g for 7 minutes at 4°C to separate live and dead hepatocytes. After washing twice, hepatocytes cells were seeded in collagen coated plate at 2.2*10e5 cells/6 well. Medium was changed after 4-hour incubation at 37°C incubator with 5% CO_2. The cells can survive for about 4 days.

Primary hepatocyte cells from B6 and DBA (n=3/strain) were subject to direct fructose treatment at 5mM and 45mM concentrations for 6, 12, 24 and 48 hours, followed by RNA isolation and qPCR for *Fgf21* and *Lss* using primers as following: *Fgf21*-F AGATCAGGGAGGATGGAACA; *Fgf21*-R TCAAAGTGAGGCGATCCATA; *Lss*-F AAACATTCAGGACAGCCAGC; *Lss*-R GCCTGATGATCCTGACCTTG. Gene expression changes in response to fructose treatment at different concentrations and time points were normalized to the baseline expression prior to fructose addition. One-way ANOVA followed by Dunnett multiple comparison correction was used to determine statistical significance in gene expression levels. For the validation of key driver gene subnetwork, we used RNAi to knockdown the key driver gene. siRNA oligos ordered from Sigma were delivered into cells using Lipofectamine RNAiMAX reagent according to the protocol. RNA was extracted 48-hour post transfection and used for reverse transcription and quantitative PCR.

Correlation between fructose DEGs and phenotypic characteristics in the three mouse strains

To assess whether the fructose DEGs were related to the phenotypes in the fructose-fed mice, we calculated the Pearson correlation between the expression n level of DEGs and the measurement of individual metabolic traits. Banjamini-Hochberg was used to control false discovery rate for multiple hypothesis testing. Adjusted *p* value less than 0.05 was considered as significant.

Relevance of fructose DEGs to human GWAS genes of cardiometabolic diseases

These genes were tested for enrichment of the fructose DEGs in our mouse study using marker set enrichment analysis (MSEA) in Mergeomics. We further curated all publicly available full GWAS summary statistics for 61 human traits/diseases from various public repositories to test if the fructose DEGs are enriched for genes associated with human diseases. For each tissue-specific DEG, we used the SNPs within a 50kb chromosomal distance as the representing SNP for that gene. The trait/disease association p-value of the SNPs obtained from each GWAS were compared to that of random sets of genes to

determine the significance of association between the signature genes and diseases in human GWAS.

Statistics

For metabolic traits, including body weight, body composition, IPGTT and lipid profiling, Two-sided Student's t test was used to perform statistical test between fructose-fed and control mice within each mouse strain. For phenotypes measured at multiple time points, two-way ANOVA was used to determine the significance of treatment and time points.

Study approval

This study was performed in accordance with National Institutes of Health Guide for the Care and Use of Laboratory Animals, USA. The experimental protocol was approved by the Chancellor's Animal Research Committee of the University of California at Los Angeles.

Results

Distinct metabolic responses of the three mouse strains in response to fructose consumption

In response to 8% fructose consumption for 14 weeks, we found significant differential metabolic responses among the three stains of mice, with DBA mice demonstrating stronger sensitivity in terms of body weight and body composition while B6 and FVB mice had stronger cholesterol alterations. Specifically, B6 and FVB showed no differences in body weight over 12 weeks (Figure 1 A, C), whilefructose-fed DBAmice gained significantly higher body weight starting from the 4th week compared to the water group (Figure 1B, D). In addition, only fructose-fed DBA mice showed significant increases in fat mass while lean mass decreased compared to control group (Figure 1E and F), and the weight of retroperitoneal white adipose tissue (rWAT), mesenteric WAT (mWAT) and subcutaneous WAT (scWAT) were significantly increased (Figure 1G). To determine whether the food intake accounted for these differences, we also measured drink and food intake weekly. Although there are increasing trend for fructose intake across the three strains, food intake decreased accordingly. Total caloric intake between groups in three strains of mice was similar (Figure 1H).

As obesity is risk factor of diabetes and could leads to insulin resistance, we analyzed the glucose tolerance of mice at different time points using IPGTT. Fructose administration caused increased area under the curve (AUC) in DBA compared to control starting the 4th week, indicating that fructose may impair the glucose homeostasis of DBA. In contrast, B6 and FVB exhibited no

difference between treatment groups at all time points (Figure 2A-C). Next, we evaluated the plasma insulin and glucose levels. No significant difference in glucose level could be observed between fructose and control in all three strains but DBA and FVB mice showed significantly elevated insulin levels in fructose-fed mice compared to controls (Figure 2D, E. These results agree with the IPGTT results that fructose predisposes mice to reduced insulin sensitivity.

Lastly, we assessed the influence of fructose consumption on lipid profiles. In contrast to the stronger obesity and diabetic related phenotypes observed in fructose fed DBA mice, lipid profile including TG, TC, HDL, LDL, UC and FFA did not change in response to fructose treatment. On the contrary, fructose increased the levels of TC, UC, HDL and LDL in B6 mice, while FVB mice receiving fructose displayed elevated TG and FFA but reduced TC, LDL and UC (Figure 2F-K). These results strongly support that mice with diverse genetic backgrounds exhibit distinct metabolic responses to fructose.

Distinct transcriptomic changes in response to fructose in metabolic tissues of diverse mouse strains

To explore the potential mechanisms underlying the differences in metabolic phenotypes among the mouse strains, we examined the transcriptomic alterations in tissues relevant to nutrient sensing, energy homeostasis, and metabolic regulation. Using RNA sequencing, we identified 578, 760 and 246 DEGs in liver tissue, and 157, 43 and 9 DEGs in hypothalamus tissue of B6, DBA and FVB mice, at a threshold of FDR < 0.05, respectively. Based on the DEG numbers, DBA liver and B6 hypothalamus tissues appear to be more sensitive to fructose, whereas the FVB mice appear to be least sensitive in both tissues.

Comparison of the DEGs within each tissue across mouse strains revealed high strain-specificity. Overall, only 15 liver DEGs (*Ppa1, Sec13, Arf4, Gstm1, Abca1, Htatip2, Cyb5b, Urad, Samm50, Abat, Ephx1, Grhpr, Id3, Gstp1 and Nudt7*) and one hypothalamus DEG (*Cd200*) overlapped across strains (Figure 3). Some of them involved in the response to xenobiotic stimulus (*Gstp1, Ephx1, Gstm1*) or organic cyclic compounds (*Abca1, Id3, Abat*). Especially, *Htatip2* is reported to modulate lipid metabolism through mediating the weight of lipid storage and oxidation [27]. *Urad* was identified as the gene encoding enzyme catalyzing uric to S-allantion. Epoxide hydrolase, which *Ephx1* belongs to, was revealed as a therapeutic target of obesity-induced colonic inflammation [28]. *Nudt7* was suggested to be involved in peroxisomal CoASH/acryl-CoA homeostasis [29]. All together, these represent the robust fructose targets that are independent of genetic backgrounds.

Functional categorization of fructose transcriptomic signature

Next, we annotated the functions of the DEGs using DAVID [24, 30] through which main biological pathways and processes affected by fructose could be determined. Among liver DEGs, B6 mice showed more pathways related with lipid and cholesterol metabolism (**Table 1**). For DBA mice, DEGs are primarily related with lipid and cholesterol metabolism and PPAR signaling pathway. Oxidation-reduction process is a common pathway in lipid metabolism, so shared by B6 and DBA. In contrast, FVB showed significant pathways related with vesicle mediated transport. With respect to the hypothalamus, only B6 mice exhibited significantly enriched pathways related to oxidative phosphorylation, Parkinson's disease and synaptic vesicle cycle. These molecular pathways partially explain the different metabolic phenotypes observed across strains.

KDA analysis

To explore how fructose induced the DEGs, we used two types of network analysis to pinpoint key regulators of fructose activities. First, we performed the key driver (KD) analysis of the fructose DEGs in each tissue. In liver tissue, the top KDs genes for B6 were found involved in sterol biosynthesis process including *Dhcr7, Fdft1, Lss, Sc4mol, Sqle, Idi1, Mum1, Pmvk, Fdps* and *Insig1* (Table 1). The top KDs for DBA included *Rtp4, Usp2, Irgm, Insig2, Fgf21, Ifit1, Arntl, Upp2* and *Cgref1*. Through inhibiting *Usp2* activity, metabolite of I3C, DIM showed suppression on high-fat diet induced obesity [31]. Absence of *Irgm* will lead to marked increase in inflammatory cytokine production [32]. As a negative regulator of SREBP, *Insig2* mediated REV-ERBalpha modulation in the expression of SREBP target genes in lipid metabolism [33]. Particularly, *Fgf21* was identified as a metabolic regulator which could effectively lower serum glucose and increase insulin sensitivity in obese mouse models. Pharmacological *Fgf21* treatment also lead to body weight loss in diet induce obesity mouse due to increased energy expenditure [13, 34] . *Itih3* and *Akr1d15* were found to be top KDs in FVB. *Itih3* is correlated with total GSH levels in the liver, indicating its role in glutathione metabolism in mice [35].

For hypothalamus, KDs were identified only among the B6 DEGs, including *Fmod, Serping1, Slc6A20, Foxc2* and *Aldh1a2*. *Foxc2* and *Fmod* were overlapped with collagen fibril organization process. *SLC6A20* is likely to play a role in the reabsorption of glycine and imino acids from the renal filtrate [36]. *Fmod* was also found to be a hypothalamic KD in our previous fructose study in a rat model. Ablation of *Fmod* lead to elevated TG, HDL, UC in the plasma, as well as FFA, lower glucose, insulin and improved insulin sensitivity [18].

As shown in Figure 4A and B, the top KDs in each tissue orchestrate numerous strain-specific DEGs and there were distinct subnetworks highlighting unique organization of DEGs from each strain. To validate the strain-specificity of KDs, we selected the B6-specific liver KD *Lss* and the DBA-specific liver KD *Fgf21*. We treated primary hepatocytes isolated from B6 and DBA directly with fructose. As shown in Figure 4C and D, *Fgf21* was particularly responsive to fructose in DBA and *Lss* was more responsive to fructose in B6. Next, we further investigate network driven by the key driver gene by siRNA. Four genes out of five chosen from the *Fgf21* network were affected after *Fgf21* was interrupted in DBA primary hepatocytes (Figure 4E). Besides, there are four out of five genes from *Lss* network were dysregulated when *Lss* was knockdown in B6 primary hepatocytes (Figure 4F). All together, these results validate our network predictions.

Relationship between DEGs and metabolic phenotypes in mouse and man

To investigate the relationships between tissue-specific DEGs and phenotypes of fructose fed mice, a correlation analysis was performed. At unadjusted $p < 0.01$, based on the number of DEGs correlated with phenotype, DBA has the most genes related with adiposity and TG in the liver and adiposity in hypothalamus, which corresponds to the distinctive body weight change in response to fructose in DBA. Although B6 has more differentially expressed genes than DBA and FVB in hypothalamus, it has very fewer genes related with metabolic phenotypes (Figure 5A). These correlations partially support strain-specific phenotypic differences among the mouse stains.

By setting the threshold of Benjamini-Hochberg adjusted p <0.05, liver DEGs showed significant correlation with adiposity in DBA and FVB mice, while no such correlations were found in C57 mice (Figure 5B-J). Among them, *St6gal1* was found downregulated in visceral adipose tissue of high-fat diet-induced obese C57 mice, further evidence suggest it has inhibitory role in adipogenesis [37]. Scd1 is a key enzyme of regulating hepatic lipid synthesis and beta-oxidation. Scd1 deficient mice are protected against obesity [38]. *Scd1*was also found as target of miR-212-5p under leucine deprivation, and inhibition of *Scd1* suppressed lipogenesis by miR-212-5p in the liver of mice and mouse primary hepatocytes [39]. Adipose specific phospholipase *Pla2g16* may function in regulating lipolysis in ob/ob and db/db knockout mice through autocrine and paracrine roles [40]. Interestingly, *Akr1a1* was revealed to play a role in protecting against CCl4-induced hepatic steatosis by restoring AsA via antioxidative property. In our study, *Akr1a1* was positively correlated with adiposity in liver tissue which is consistent with no changes of body weight in FVB mice [41]. In vitro study showed that *Rkip* (also known as *Pebp1*) knockdown elevated PPARgamma, resulted in stimulation of adipogenic lipid accumulation in 3T3-L1 preadipocytes overexpressing LC3 [42]. This also indicates *Rkip* may prevent against obesity which is corresponding to our FVB response to fructose treatment. Overexpression of *Glo1*, member of glyoxalase system, suppressed gain in body weight and adiposity in HFD-fed mice compared wild-type HFD-fed controls [43]. In our study, *Glo1* was positively correlated with adiposity in FVB mice, which may contribute to the resistance to body weight gain. Besides, some liver DEGs were found significantly correlated with LDL in liver of FVB. *Aldh2* variant was inversely associated with LDL cholesterol level in Japanese men consuming alcohol [44]. Reduced expression of *Enho* mRNA is reported to be associated with chronic high-fat diet, indicating deregulation of liver *Enho* expression with obesity [45]. *Svip* has been revealed to play a role in VLDL trafficking from endoplasmic reticulum to Golgi [46]. However, no correlations between DEGs and any traits could be observed in fructose fed B6 mice.

To identify genes that may have a causal role in human diseases, we performed GWAS enrichment analysis using the Mergeomic pipeline. Metabolic syndrome, cardiovascular diseases and metabolic diseases related GWAS studies (LDL, TC, CAD, HDL, TG, Obesity and T2D) were incorporated into the enrichment analysis. In liver tissue, we observed significant enrichment for overlapping genes between fructose signature and top GWAS hits for HDL, LDL and TG in three strains. In hypothalamus, only GWAS hits for TG and TC were found significantly overlapped with gene signature in B6, rather than the other strains. These results indicate that the fructose-affected genes are highly relevant to human disease biology.

Discussion

In this study we demonstrated that in response to physiologically relevant doses of fructose, phenotypic and transcriptomic differences exist among mice of different genetic strains and we explored the genes and pathways that may potentially explain the molecular mechanisms behind such differences. Our findings are in line with prior studies that showed strain-specific responses to other diets such as high fat high sucrose diet (HFHS) and a high calorie diet [14]. Interestingly, the patterns of phenotypic differences are not only strain-specific but also diet-specific. For example, when comparing the B6, DBA, and FVB mouse strains, B6 mice gained the most weight when fed HFHS diet [14], whereas in our study, DBA mice gained the most weight when fed fructose diet. This diet-specific variability across strains indicates different adaptive abilities of different genetic background towards different diets.

Our transcriptomic studies provide clues to the potential molecular underpinnings of the differential metabolic responses to fructose in the three mouse strains. In particular, we found very limited overlap between strains in the tissue-specific DEGs altered by fructose. Liver-specific DEGs were enriched for the PPAR signaling pathway in the DBA mouse strain alone. This finding may explain why DBA was the only mouse strain to gain weight and fat mass in response to fructose. Indeed, we see a similar effect in humans where weight gain is a common side effect of thiazolidinediones, a PPAR gamma agonist commonly used to treat type 2 diabetes. Network modeling revealed *Fgf21* to be a DBA-specific key regulator in the liver in response to fructose. FGF21 is a novel hormone that holds promise as potential therapy for type 2 diabetes. It is primarily produced by the liver, where its expression is partially under the control of the transcription factor PPARα. Transgenic mice overexpressing FGF21 are protected against diet-induced obesity, while mice in which FGF21 is ablated exhibit increased weight gain and impaired glucose tolerance when placed on a high-fat diet (HFD). Furthermore, several lines of evidence suggest that FGF21 regulates hyperglycemia, at least in part, via the sensitization of insulin action, an effect we hypothesized is mediated by the liver. In obese animals, FGF21 lowers both glucose and insulin levels, suggesting an

improvement in insulin sensitivity. In our study we found that in DBA mice, *Fgf21* is significantly reduced by fructose, which agrees with the compromised glucose homeostasis and increased adiposity observed. Our in vitro fructose treatment experiments in primary hepatocytes confirmed that *Fgf21* is a direct and acute target of fructose in hepatocytes, and agreeing with our in vivo data and network analysis, the response of *Fgf21* is most significant in DBA. There is also an interesting directional shift in *Fgf21* between the acute fructose response in primary hepatocytes where *Fgf21* immediately increases upon fructose treatment at early time points, whereas in our long-term (12-week) in vivo treatment study *Fgf21* is inhibited by fructose most significantly in DBA. Perhaps *Fgf21* is an early homeostatic regulator which quickly responds to fructose at the beginning but upon long-term exposure, fructose or fructose metabolites or other downstream effectors inhibit *Fgf21*.

In FVB mice, fructose induced transcriptomic changes in the liver involving vesicle-mediated transport pathways which may be the mechanism underlying the decrease in plasma cholesterol and LDL levels in response to fructose (in the other strains, these levels either increased or did not change). It is well established that LDL in the plasma binds to its receptor on the surface of hepatocytes and subsequently undergoes receptor-mediated endocytosis for downstream intracellular processing. However the intracellular trafficking pathways of cholesterol in hepatocytes are poorly defined [47] and the potential link between such pathways and the altered LDL and cholesterol levels in our FVB fructose-fed mice warrants further investigation. Further exploration of the fructose gene signature in FVB mice revealed that *Nat2*, a potentially causal gene in human cardiometabolic disease, may also have an important role in rodents. *Nat2* encodes the enzyme N-acetyltransferase 2 which acetylates arylamine and hydrazine drugs and carcinogens. In human GWAS, a nonsynonymous SNP in NAT2 was nominally associated with various cardiometabolic traits including TG, TC and LDL levels. Furthermore, mice deficient in Nat1, an ortholog of Nat2, had elevations in insulin and triglycerides [48]. These observations are consistent with the phenotypic response FVB mice had to fructose in our study.

In the hypothalamus, fructose induced the strongest transcriptomic changes in B6 mice compared to the other two strains (~400 DEGs compared to ~100 and ~20) and network analysis revealed the extracellular matrix gene *Fmod* as the top key driver. This is consistent with our prior study which also found Fmod to be a key regulator in the rat hypothalamus in response to fructose consumption, and we validated this finding in a *Fmod* knockout mouse model which showed significantly higher levels of TG, TC, UC, HDL compared to wild type mice in response to fructose [18]. In the current study, only the B6 strain similarly had a significant increase in TC, UC, HDL, and LDL in response to fructose suggesting that *Fmod* as a key regulatory gene may be strain-specific. These B6-specific increases in cholesterol in response to fructose could also be related to dysregulation of *Lss*, a key regulatory gene revealed in our network analysis of B6 liver DEGs. *Lss* encodes lanosterol synthase which converts (S)-2,3 oxidosqualene to lanosterol, a key intermediate in cholesterol biosynthesis. Thus, there is growing interest in targeting this enzyme therapeutically to lower blood cholesterol (PMID 28462697?)

In addition to the distinct DEGs and pathways across strains, our transcriptomic analysis also revealed certain shared fructose DEGs across strains, which may imply robust targets of fructose regardless of genetic background. The 15 shared DEGs in the liver were enriched for genes known to be downregulated in hepatocellular carcinoma and genes that are known targets of proto-oncogene Myc. The only shared DEG in the hypothalamus was *Cd200* which encodes a type 1 membrane glycoprotein belonging to the immunoglobulin superfamily. It plays an important role in immunosuppression and regulation of anti-tumor activity (genecards.org). The potential role of fructose in malignancy is an important question and deserves further investigation.

The strengths of our study include the use of three different strains of mice in three parallel fructose vs control models to investigate the potential role of genetic background in the response to fructose. We comprehensively characterized both metabolic parameters and transcriptomic alterations to make potential links and comparisons between phenotype and molecular perturbations across different genetic strains.

The limitation of our study is the use of RNA sequencing of bulk tissue. Thus, while we are able to investigate the molecular response of fructose in liver and hypothalamus

tissues as a whole, we were unable to resolve potential causal cell types and cell-cell interactions without the use of single-cell RNA sequencing. We plan to explore the in vivo response of fructose at single cell resolution in future studies.

In conclusion, we demonstrated that fructose induces distinct metabolic phenotypes and molecular signatures in mice of different genetic strains. With the exponential rise of fructose consumption and concomitant increase in obesity and metabolic syndrome, it is important to better understand whether and how individuals differ in their response to fructose consumption. Our study provides a step forward in this direction with a goal of developing personalized preventive and therapeutic strategies.

References

1. Lakka, H.M., et al., *The metabolic syndrome and total and cardiovascular disease mortality in middle-aged men.* JAMA, 2002. **288**(21): p. 2709-16.
2. Vanni, E., et al., *From the metabolic syndrome to NAFLD or vice versa?* Dig Liver Dis, 2010. **42**(5): p. 320-30.
3. Te Morenga, L., S. Mallard, and J. Mann, *Dietary sugars and body weight: systematic review and meta-analyses of randomised controlled trials and cohort studies.* BMJ, 2012. **346**: p. e7492.
4. Yang, Q., et al., *Added sugar intake and cardiovascular diseases mortality among US adults.* JAMA Intern Med, 2014. **174**(4): p. 516-24.
5. Jayalath, V.H., et al., *Total fructose intake and risk of hypertension: a systematic review and meta-analysis of prospective cohorts.* J Am Coll Nutr, 2014. **33**(4): p. 328-39.
6. Stanhope, K.L., et al., *Consuming fructose-sweetened, not glucose-sweetened, beverages increases visceral adiposity and lipids and decreases insulin sensitivity in overweight/obese humans.* J Clin Invest, 2009. **119**(5): p. 1322-34.
7. Te Morenga, L.A., et al., *Dietary sugars and cardiometabolic risk: systematic review and meta-analyses of randomized controlled trials of the effects on blood pressure and lipids.* Am J Clin Nutr, 2014. **100**(1): p. 65-79.
8. Bray, G.A., S.J. Nielsen, and B.M. Popkin, *Consumption of high-fructose corn syrup in beverages may play a role in the epidemic of obesity.* Am J Clin Nutr, 2004. **79**(4): p. 537-43.
9. Malik, V.S., et al., *Sugar-sweetened beverages and risk of metabolic syndrome and type 2 diabetes: a meta-analysis.* Diabetes Care, 2010. **33**(11): p. 2477-83.
10. Dhingra, R., et al., *Soft drink consumption and risk of developing cardiometabolic risk factors and the metabolic syndrome in middle-aged adults in the community.* Circulation, 2007. **116**(5): p. 480-8.
11. Cox, C.L., et al., *Consumption of fructose-sweetened beverages for 10 weeks reduces net fat oxidation and energy expenditure in overweight/obese men and women.* Eur J Clin Nutr, 2012. **66**(2): p. 201-8.
12. Cox, C.L., et al., *Consumption of fructose- but not glucose-sweetened beverages for 10 weeks increases circulating concentrations of uric acid, retinol binding protein-4, and gamma-glutamyl transferase activity in overweight/obese humans.* Nutr Metab (Lond), 2012. **9**(1): p. 68.
13. Glendinning, J.I., et al., *Differential effects of sucrose and fructose on dietary obesity in four mouse strains.* Physiol Behav, 2010. **101**(3): p. 331-43.
14. Parks, B.W., et al., *Genetic control of obesity and gut microbiota composition in response to high-fat, high-sucrose diet in mice.* Cell Metab, 2013. **17**(1): p. 141-52.
15. Morton, G.J., et al., *Central nervous system control of food intake and body weight.* Nature, 2006. **443**(7109): p. 289-95.
16. Coll, A.P., I.S. Farooqi, and S. O'Rahilly, *The hormonal control of food intake.* Cell, 2007. **129**(2): p. 251-62.

17. Minokoshi, Y., et al., *AMP-kinase regulates food intake by responding to hormonal and nutrient signals in the hypothalamus.* Nature, 2004. **428**(6982): p. 569-74.
18. Meng, Q., et al., *Systems Nutrigenomics Reveals Brain Gene Networks Linking Metabolic and Brain Disorders.* EBioMedicine, 2016. **7**: p. 157-66.
19. Nomura, K. and T. Yamanouchi, *The role of fructose-enriched diets in mechanisms of nonalcoholic fatty liver disease.* J Nutr Biochem, 2012. **23**(3): p. 203-8.
20. Pertea, M., et al., *Transcript-level expression analysis of RNA-seq experiments with HISAT, StringTie and Ballgown.* Nat Protoc, 2016. **11**(9): p. 1650-67.
21. Kim, D., B. Langmead, and S.L. Salzberg, *HISAT: a fast spliced aligner with low memory requirements.* Nat Methods, 2015. **12**(4): p. 357-60.
22. Pertea, M., et al., *StringTie enables improved reconstruction of a transcriptome from RNA-seq reads.* Nat Biotechnol, 2015. **33**(3): p. 290-5.
23. Frazee, A.C., et al., *Ballgown bridges the gap between transcriptome assembly and expression analysis.* Nat Biotechnol, 2015. **33**(3): p. 243-6.
24. Huang da, W., B.T. Sherman, and R.A. Lempicki, *Systematic and integrative analysis of large gene lists using DAVID bioinformatics resources.* Nat Protoc, 2009. **4**(1): p. 44-57.
25. Arneson, D., et al., *Mergeomics: a web server for identifying pathological pathways, networks, and key regulators via multidimensional data integration.* BMC Genomics, 2016. **17**(1): p. 722.
26. Shannon, P., et al., *Cytoscape: a software environment for integrated models of biomolecular interaction networks.* Genome Res, 2003. **13**(11): p. 2498-504.
27. Liao, B.M., et al., *Proteomic analysis of livers from fat-fed mice deficient in either PKCdelta or PKCepsilon identifies Htatip2 as a regulator of lipid metabolism.* Proteomics, 2014. **14**(21-22): p. 2578-87.
28. Wang, W., et al., *Lipidomic profiling reveals soluble epoxide hydrolase as a therapeutic target of obesity-induced colonic inflammation.* Proc Natl Acad Sci U S A, 2018. **115**(20): p. 5283-5288.
29. Reilly, S.J., et al., *The nudix hydrolase 7 is an Acyl-CoA diphosphatase involved in regulating peroxisomal coenzyme A homeostasis.* J Biochem, 2008. **144**(5): p. 655-63.
30. Huang da, W., B.T. Sherman, and R.A. Lempicki, *Bioinformatics enrichment tools: paths toward the comprehensive functional analysis of large gene lists.* Nucleic Acids Res, 2009. **37**(1): p. 1-13.
31. Yang, H., et al., *3,3'-Diindolylmethane suppresses high-fat diet-induced obesity through inhibiting adipogenesis of pre-adipocytes by targeting USP2 activity.* Mol Nutr Food Res, 2017. **61**(10).
32. Schmidt, E.A., et al., *Metabolic Alterations Contribute to Enhanced Inflammatory Cytokine Production in Irgm1-deficient Macrophages.* J Biol Chem, 2017. **292**(11): p. 4651-4662.
33. Le Martelot, G., et al., *REV-ERBalpha participates in circadian SREBP signaling and bile acid homeostasis.* PLoS Biol, 2009. **7**(9): p. e1000181.

34. Xu, J., et al., *Acute glucose-lowering and insulin-sensitizing action of FGF21 in insulin-resistant mouse models--association with liver and adipose tissue effects.* Am J Physiol Endocrinol Metab, 2009. **297**(5): p. E1105-14.
35. Wickramasekara, R.N., et al., *Glutathione and Inter-alpha-trypsin inhibitor heavy chain 3 (Itih3) mRNA levels in nicotine-treated Cd44 knockout mice.* Toxicol Rep, 2018. **5**: p. 759-764.
36. Thwaites, D.T. and C.M. Anderson, *The SLC36 family of proton-coupled amino acid transporters and their potential role in drug transport.* Br J Pharmacol, 2011. **164**(7): p. 1802-16.
37. Kaburagi, T., et al., *The Inhibitory Role of alpha2,6-Sialylation in Adipogenesis.* J Biol Chem, 2017. **292**(6): p. 2278-2286.
38. Ntambi, J.M., et al., *Loss of stearoyl-CoA desaturase-1 function protects mice against adiposity.* Proc Natl Acad Sci U S A, 2002. **99**(17): p. 11482-6.
39. Guo, Y., et al., *miR-212-5p suppresses lipid accumulation by targeting FAS and SCD1.* J Mol Endocrinol, 2017. **59**(3): p. 205-217.
40. Jaworski, K., et al., *AdPLA ablation increases lipolysis and prevents obesity induced by high-fat feeding or leptin deficiency.* Nat Med, 2009. **15**(2): p. 159-68.
41. Akihara, R., et al., *Ablation of aldehyde reductase aggravates carbon tetrachloride-induced acute hepatic injury involving oxidative stress and endoplasmic reticulum stress.* Biochem Biophys Res Commun, 2016. **478**(2): p. 765-71.
42. Hahm, J.R., M. Ahmed, and D.R. Kim, *RKIP phosphorylation-dependent ERK1 activation stimulates adipogenic lipid accumulation in 3T3-L1 preadipocytes overexpressing LC3.* Biochem Biophys Res Commun, 2016. **478**(1): p. 12-17.
43. Rabbani, N. and P.J. Thornalley, *Glyoxalase 1 Modulation in Obesity and Diabetes.* Antioxid Redox Signal, 2018.
44. Tabara, Y., et al., *Mendelian randomization analysis in three Japanese populations supports a causal role of alcohol consumption in lowering low-density lipid cholesterol levels and particle numbers.* Atherosclerosis, 2016. **254**: p. 242-248.
45. Kumar, K.G., et al., *Identification of adropin as a secreted factor linking dietary macronutrient intake with energy homeostasis and lipid metabolism.* Cell Metab, 2008. **8**(6): p. 468-81.
46. Tiwari, S., et al., *Silencing of Small Valosin-containing Protein-interacting Protein (SVIP) Reduces Very Low Density Lipoprotein (VLDL) Secretion from Rat Hepatocytes by Disrupting Its Endoplasmic Reticulum (ER)-to-Golgi Trafficking.* J Biol Chem, 2016. **291**(24): p. 12514-26.
47. Maxfield, F.R. and D. Wustner, *Intracellular cholesterol transport.* J Clin Invest, 2002. **110**(7): p. 891-8.
48. Knowles, J.W., et al., *Identification and validation of N-acetyltransferase 2 as an insulin sensitivity gene.* J Clin Invest, 2015. **125**(4): p. 1739-51.

Tables.

Table 1. Summary of DEGs in liver and hypothalamus tissues of three mouse strains at FDR<0.05.

Tissue	strain	DEG No.	Top 5 pathways	Top KDs	GWAS traits (genes whose SNPs with GWAS p value <1e-8)
liver	B6	578	Oxidation-reduction process, Metabolic pathways, Lipid metabolic process, Biosynthesis of antibiotics, Cholesterol metabolic process	*Dhcr7, Fdft1, Lss, Sc4mol, Sqle*	**HDL** (FADS2, NDUFB10, NDUFS3, PABPC4, PLTP, SLC39A8) **LDL** (FADS2, HIST1H4H, HP) **Triglyceride** (FADS2, PLTP, PABPC4) TC (HP, FADS2) **CAD** (USMG5) **Fasting glucose** (NOSTRIN, FADS2, KHK)
	DBA	760	Oxidation-reduction process, Metabolic pathways, Lipid metabolic process, PPAR signaling pathway, Fatty acid metabolic process	*Rtp4, Usp2, Irgm, Insig2, Fgf21*	**HDL** (LIPC, LIPG, NFATC3, LRP4, DDB1, ANGPTL4, PSMA5, AMFR) **LDL** (PSMA5, DDB1, ANGPTL3, DDX56, GSTM4, UGT1A1, ACADS) **Triglycerides** (ANGPTL3, DDB1, LIPC, LRPAP1, HDAC11) **Total cholesterol** (ANGPTL3, DDB1, DDX56, GSTM4, LIPC, LIPG, LR, PAP1, UGT1A1) **CAD** (PSMA5) **Fasting glucose** (NOSTRIN, DDB1)
	FVB	246	vesicle-mediated transport, protein transport, Metabolic pathways, oxidation-reduction process, Chemical carcinogenesis	*Itih3, Akr1d1*	**HDL** (PSMA5, DNTTIP1) **LDL** (PSMA5, ANGPTL3, GSTM4) **Triglycerides** (ANGPTL3, NAT2, STK19, DNTTIP1) **Total cholesterol** (PSMA5, ANGPTL3, NAT2, GSTM4) **CAD** (PSMA5, GGCX)
Hypothalamus	B6	484	Ribosome, Translation, Transport, Oxidative phosphorylation, regulation of sensory perception of pain	*Fmod, Gpr81, Aldh1a2, Serping1, Slc22a6*	**Triglycerides** (LRPAP1) **Total cholesterol** (CPNE1, LRPAP1)
	DBA	119	Protein processing in endoplasmic reticulum, reactive oxygen species metabolic process, protein folding, histone H3-K27 trimethylation, nucleosome positioning	None	None
	FVB	25	RNA secondary structure unwinding, negative regulation of apoptotic process	None	None

Table 2. Relationship between gene expression and phenotype using Pearson correlation

Tissue	**Strain**	**Phenotype**	**Gene correlated with phenotype at corrected p < 0.05**
Liver	DBA	Adiposity	*Sult1c2, Abca8a, Hist1h1d, Aatf, Ap4s1, St6gal1, Scd1, Pla2g16, Mx2, Igtp, Rtn4, Parp14*
	FVB	Adiposity	*Txn1, Akr1a1, Galk1, 5031425E22Rik, Gss, Ctsz, Gm38426, Gstm1, Adi1, Dnajc22, Fam213b, Gstm4, Urad, Scarna10, Renbp, Atp5g3, Atp5g2, Akr1c13, Tmem14c, H2afz, Pebp1, Ugt2b34, Ces2a, Atox1, Aldh2, Ppp1r2, Uqcr10, Cbr1, Gstp1, Glo1, Psma1, Abhd11, Rtn4, Tkt, Cyp2c70, Gm3219, Pcp4l1, Srp72, Serpinf2, 4933434E20Rik, F12, Psmd12, Psma5, C2cd2, Slc25a5, Pfkm, Rps14, Enho, Lancl1, Stt3a, Ccl9, App, Jun, Npc2, Wfdc21, Gstt1*
		Insulin	*Id3*
		LDL	*Btg2, Dnttip1, Fam120aos, Psmd12, Psma1, Serpinf2, Eef1d, Txnl1, Uqcr10, Tmem14c, Psma5, Sbds, Aldh2, Cyp2c70, Ctsz, Cblc, Apon, Enho, Dnajc22, Adi1, Svip, Cox5a, C77080, Inpp1, F12, Akr1c13, 2810013P06Rik, Psmd14, Rpl14*
Hypothalamus	DBA	Adiposity	*Slc38a2, Hist1h1e, Aifm3, Slc6a8, Npcd, Tmem170b, Mat2a*
	FVB	UC	*Ddx3x*

Figures

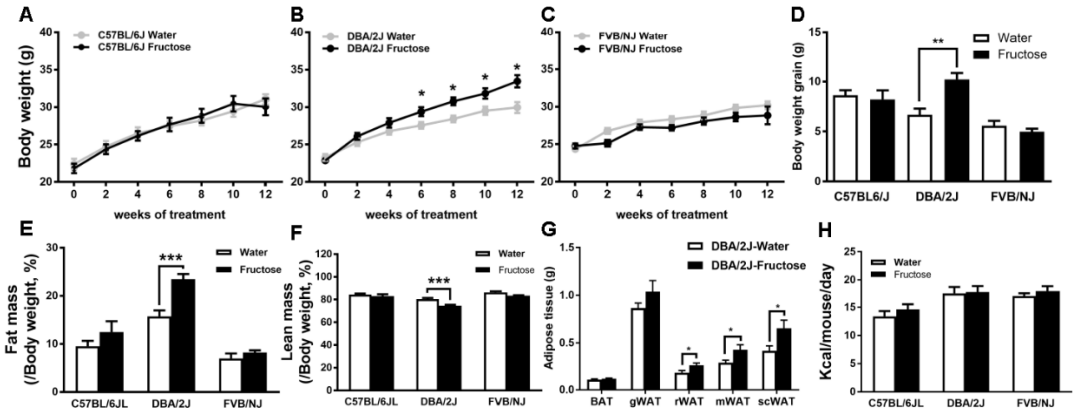

Figure 1. Body weight and composition changes in three strains of mice. Cumulative change in body weight in B6 (A), DBA (B) and FVB (C) mice fed normal Chow diet with water or 8% fructose over 12 weeks and body weight gain (D) at the end of experiment. Body composition change in three strains of mice. Fat mass (E), lean mass (F), adipose tissue of DBA (G) were measured using NMR and food intake (H) of three stains of mice. Error bars in the graph are standard errors. * denotes $p < 0.05$ and ** denotes $p < 0.01$ by two-sided Student's t-test.

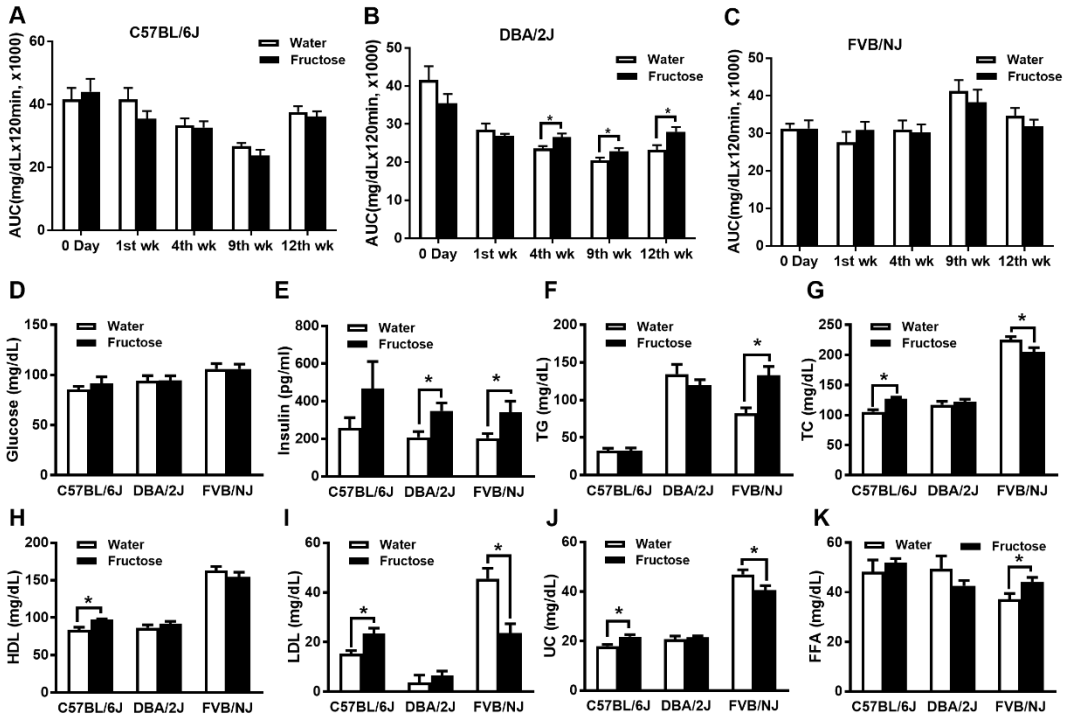

Figure 2. Glucose metabolism and lipid profiling in three strains of mouse at different time points. Glucose analysis using IPGTT were conducted at baseline (0 day), 1st, 4th,9thand 12th week shown as area under the curve (AUC) (A-C). Plasma glucose (D), insulin (E), triglyceride (F), total cholesterol (G), HDL (H), LDL (I), unesterified cholesterol (J) and free fatty acid (K) levels are shown (n=8-10 per group). *$p < 0.05$ and **$p < 0.01$ by two-sided Student's t-test.

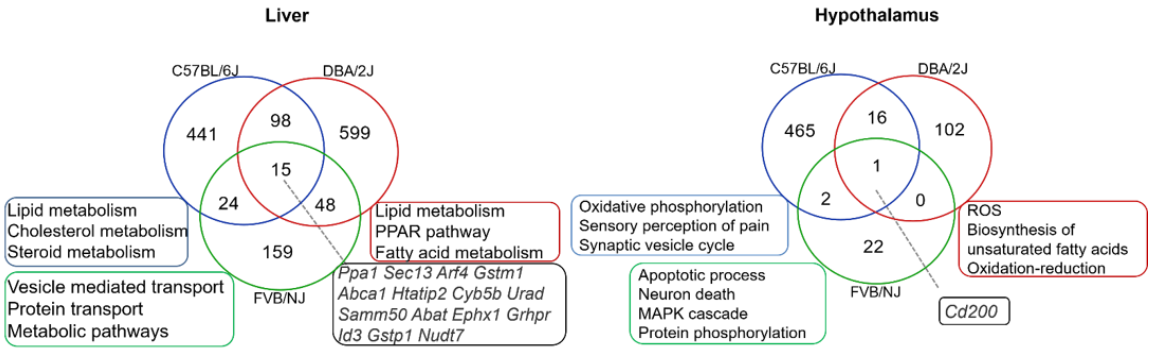

Figure 3. Venn diagram of DEGs across different tissues, liver and hypothalamus of three strains of mice

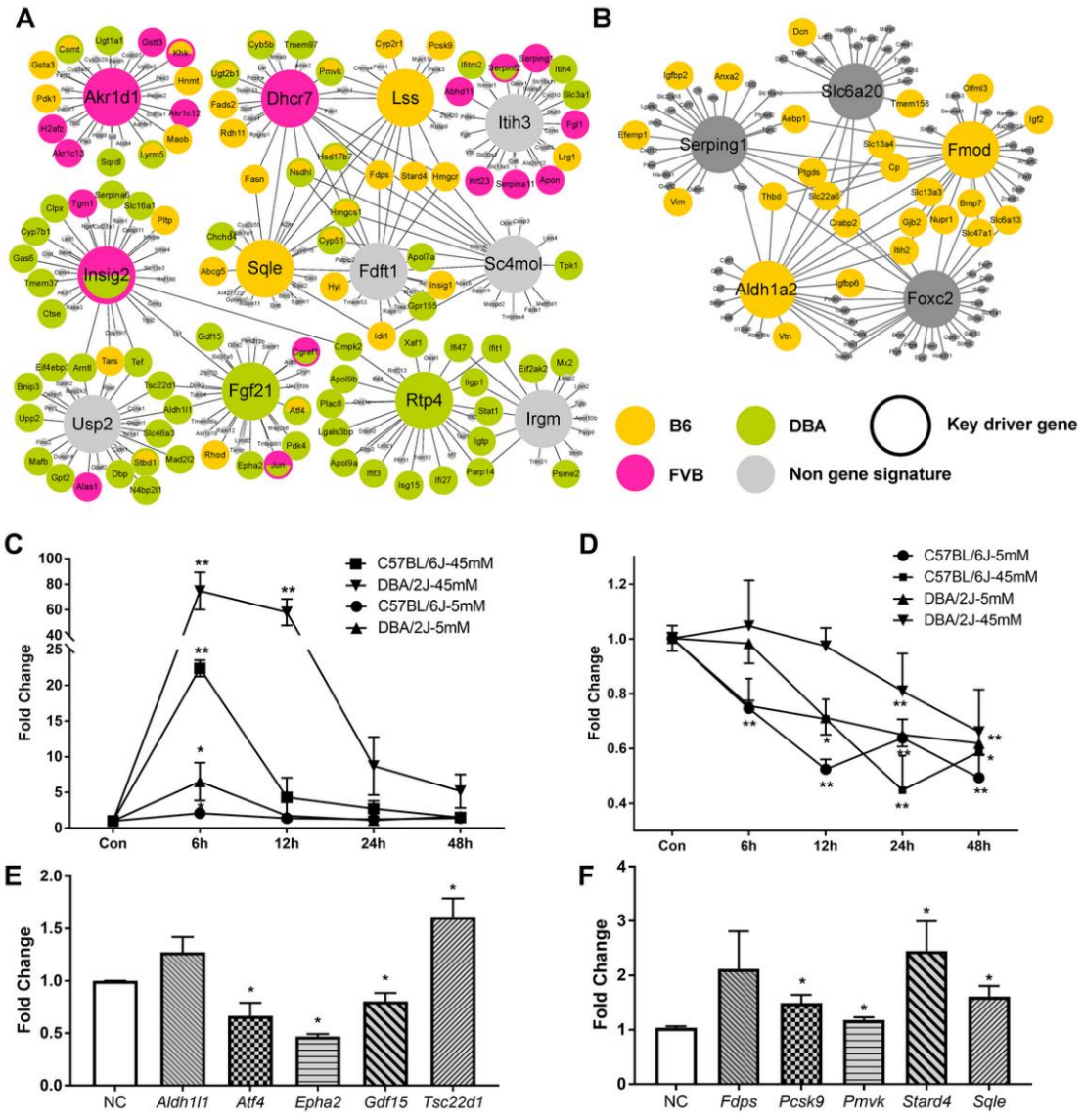

Figure 4. Gene subnetworks and top network key drivers (KDs) of three strains of mice receiving fructose and validation of select strain-specific liver KDs in primary hepatocytes. (A) Liver KDs and subnetworks. (B) Hypothalamus KDs and subnetworks. (C) Direct response to fructose for DBA-specific KD *Fgf21* is stronger in DBA than in B6. (D) Direct response to fructose for B6-specific KD *Lss* is stronger in B6 than in DBA. *$p < 0.05$ and **$p < 0.01$ by one-way ANOVA. (E) Expression changes of genes in *Fgf21* driven network after knockdown of *Fgf21* in DBA primary hepatocytes. (F) Expression changes of genes in *Lss* driven network after knockdown of *Lss* in B6 primary hepatocytes. *$p < 0.05$ and **$p < 0.01$ by two-sided Student's t-test.

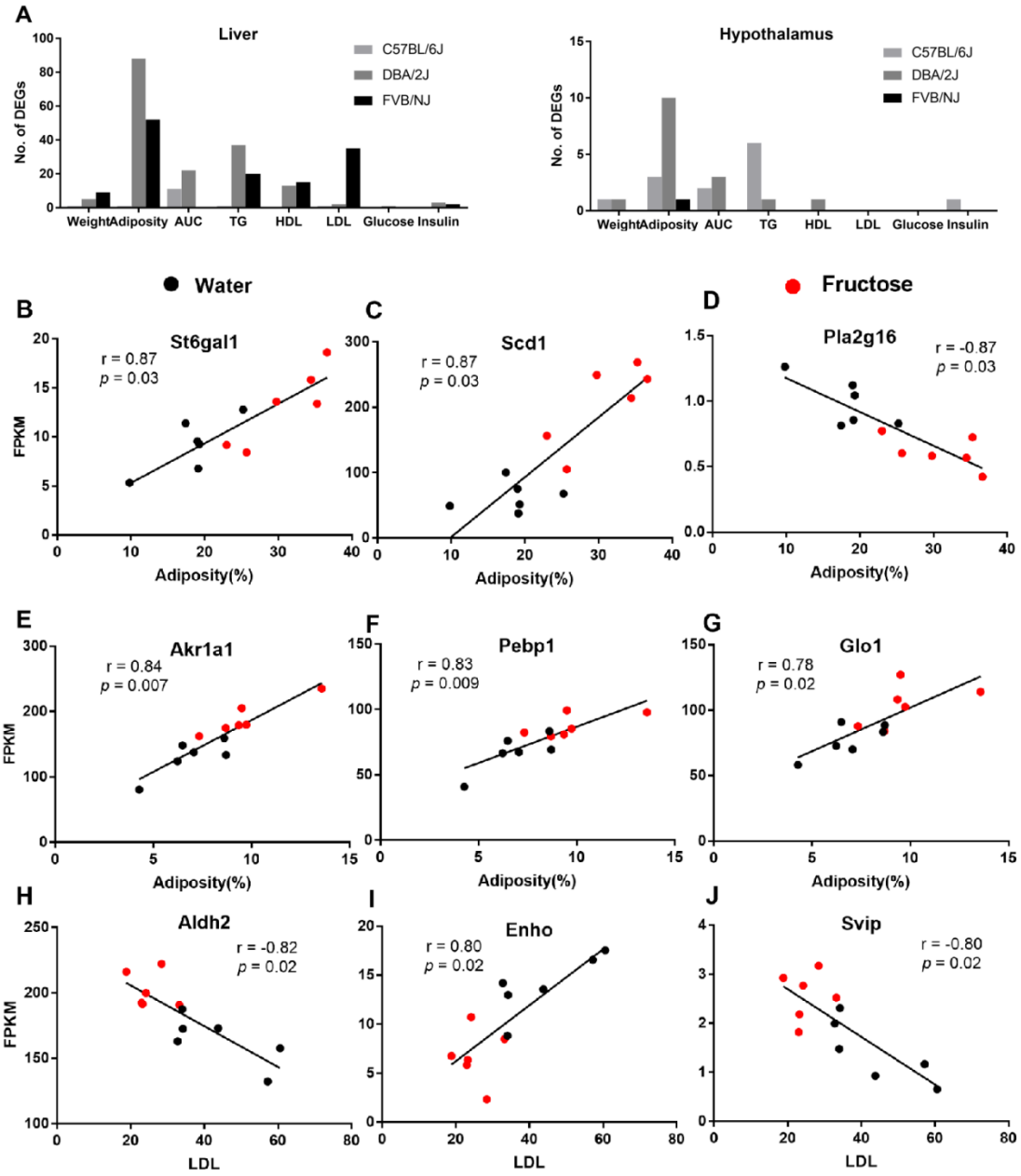

Figure 5. Relationship between DEGs and metabolic traits in mouse. (A) Number of strain-specific DEGs that are correlated with metabolic traits in our fructose study ($p < 0.01$). (B-D) Select examples of DEGs in liver correlating with adiposity in DBA mice. (E-G) Select examples of DEGs in liver correlating with adiposity in FVB mice. (H-J) Select examples of DEGs in liver correlating with LDL in FVB mice.

Acknowledgements

X.Y. and F.G-P. are funded by R01 DK104363 and R21 NS103088. F.GP. is funded by R01 NS50465 and UCLA BIRC.